ACS OMEGA

http://pubs.acs.org/journal/acsodf

Article

# Flexible and Conductive Polymer Threads for Efficient Fiber-Shaped Supercapacitors *via* Vapor Copolymerization

Jing Hu, Bo Gao, Qi Qi, Zhuang Zuo, Kai Yan, Shaocong Hou,* and Dechun Zou*

Cite This: *ACS Omega* 2022, 7, 31628−31637

Read Online

ACCESS | Metrics & More | Article Recommendations | Supporting Information

**ABSTRACT:** Flexible fiber electrodes are critical for high-performance fiber and wearable electronics. In this work, we presented a highly conductive all-polymer fiber electrode by vapor copolymerization of 2,5-dibromo-3,4-vinyldioxythiophene (DBE-DOT) and 2,5-diiodo-3,4-vinyldioxythiophene (DIEDOT) monomers on commonly used polyester threads (PETs) at a temperature as low as 80 °C. The poly(3,4-ethylenedioxythiophene) (PEDOT)-coated PET threads maintain excellent flexibility and show conductivity of 7.93 S $cm^{-1}$, nearly four times higher than that reported previously *via* homopolymerization of DBEDOT monomer. A $MnO_2$ active layer was embedded into the PEDOT double layers, and the flexible fiber composite electrode showed a high linear specific capacitance of 157 mF $cm^{-1}$ and improved stability, retaining 86.5% capacitance after 5000 cycles. Fiber-shaped solid-state supercapacitors (FSSCs) based on the composite electrodes were assembled, and they displayed superior electrochemical performance. This work provides a new approach to realize high-performance and stable wearable electronics.

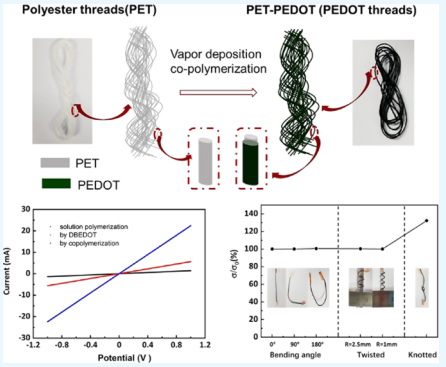


## 1. INTRODUCTION

In recent years, flexible and wearable electronics have become important technological trends and experienced rapid growth. Wearable electronic devices often rely on energy storage units to provide a continuous energy supply and sufficient power density.[1−3] Among all of the existing energy storage solutions, flexible electrochemical supercapacitors with a fast charge−discharge rate, high power density, and superior stability are desirable for wearable electronics.[1,4] One of the attractive approaches to realize flexible supercapacitors is developing fiber-shaped supercapacitors (FSSCs). Compared to planar supercapacitors, FSSCs have a smaller volume and excellent flexibility and, most importantly, can be woven into textiles, which is ideal for wearable applications.[5−7]

Flexible and conductive fiber electrodes are essential components for FSSCs. High conductivity can facilitate electron transportation and electrochemical reaction inside the electrode, thus helping to achieve high rate ability and increase the stability of devices. Metal wires[8−10] and carbon fibers[11−13] with high conductivity have been widely used as electrodes, while their flexibility is inferior. Alternatively, low-cost and light-weight polymer fibers, such as polyester threads and cotton threads commonly used in textile and cloth, are flexible and wearable, however requiring external conductive coatings on the fiber substrates.[14,15] The coating processes on polymer substrates have to be conducted at low temperatures due to their low glass transition and decomposition temperatures. Liu et al.[15] reported Ni-coated cotton fibers by electroless deposition with reduced graphene oxide (rGO) nanosheets for supercapacitors. Liu et al.[16] developed single-wall carbon nanotube-modified cotton threads by the dip-coating method. Besides metal and carbon materials, conductive polymers are also used to modify textile electrodes. Wei et al.[17] prepared polypyrrole nanotube-coated cotton yarns *via* in situ polymerization for supercapacitors and achieved a high areal specific capacitance of 74.0 mF $cm^{-2}$. Poly(3,4-ethylenedioxythiophene) (PEDOT)-coated fiber electrodes were also reported by coating poly(3,4-ethylenedioxythiophene)/poly(styrene sulfonate) (PEDOT:PSS) dispersive solution[18] or oxidative polymerization in solution.[19] However, the adhesion between the active materials and substrates is weak, leading to a compromise between conductivity and mechanical property.

To address these problems, vapor polymerization combining vapor deposition of monomers and in situ polymerization has been proposed.[20] Small-molecule monomers in vapor state can penetrate into the microscopic pores of the fiber substrates under the reduced pressure condition and thus form a continuous and robust conductive layer on fibers after polymerization. For example, Andrew's group developed oxide chemical vapor deposition (oCVD) of conductive polymers on fiber and textile substrates;[21] however, metal

Received: October 12, 2021
Accepted: February 18, 2022
Published: September 3, 2022





https://doi.org/10.1021/acsomega.1c05717
*ACS Omega* 2022, 7, 31628−31637

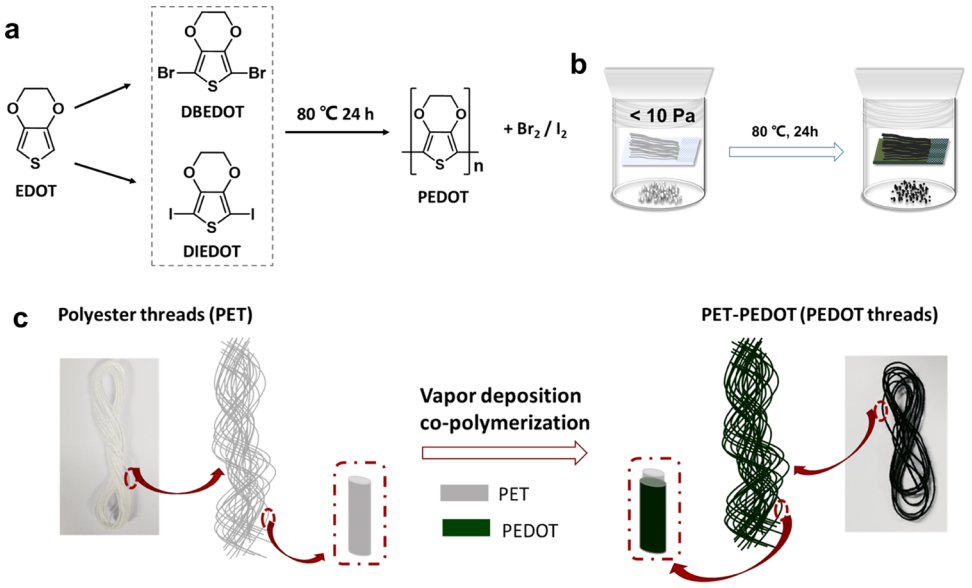


**Figure 1.** (a) Chemical reaction process of monomer synthesis and polymerization and (b) schematic figure of the vapor deposition polymerization device and process. (c) Photo image and the schematic diagram of polyester threads before and after PEDOT deposition.

catalysts required to initiate the polymerization are difficult to be removed after the reaction. Meng et al.[22,23] and our group[24,25] reported vapor homopolymerization of 2,5-dibromo-3,4-ethylenedioxythiophene (DBEDOT) monomer, which could undergo an in situ self-catalyzed reaction at a mild temperature (80 °C) below the glass transition temperature of polymer substrates. However, the conductivity of PEDOT polymerized from DBEDOT is still moderate (less than 2 S $cm^{-1}$ based on the whole electrode), which limits the rate ability and electrochemical performance in supercapacitors.

In this work, we synthesized 2,5-diiodo-3,4-vinyldioxythiophene (DIEDOT) and studied its copolymerization behavior with DBEDOT at a mild temperature for the first time. The resulting bromine- and iodine-co-doped PEDOT-modified polyester thread showed a conductivity of 7.93 S $cm^{-1}$, nearly four times higher than that obtained when prepared by DBEDOT polymerization alone. In addition, the co-doped PEDOT threads also showed excellent flexibility and stability, and no change of conductivity was observed at different bending angles. Moreover, the PEDOT-modified polyester thread was further deposited with $MnO_2$ by electrodeposition, showing linear specific capacitance of 157 mF $cm^{-1}$ and areal specific capacitance of 772 mF $cm^{-2}$ at a discharge current of 0.3 mA $cm^{-1}$ (1.47 mA $cm^{-2}$). These results showed that the vapor deposition of PEDOT copolymerized by DBEDOT and DIEDOT provided a promising way to prepare electrodes with excellent electrochemical and mechanical properties for flexible electronic devices.

## 2. RESULTS AND DISCUSSION

Figure 1a shows the halide substitution reaction of EDOT monomers, followed by vapor polarization. DIEDOT monomer formed white crystals after iodide substitution and purification. Meng et al.[23] predicated that closely packed DIEDOT monomers in the crystal could undergo cross-coupling polymerization self-catalyzed by the product of $I_2$ similar to DBEDOT, but the temperature was required to be above 140 °C, which indicates that iodine-substituted DIEDOT is much less reactive than the bromine-substituted one (DBEDOT). The high polymerization temperature of DIEDOT monomer could not polymerize to PEDOT completely at 80 °C, limiting its application in temperature-sensitive substrates, such as poly(ethylene terephthalate) (PET) fibers (glass temperature of 81 °C).

Copolymerization is an important approach to change the reaction dynamics and the properties of polymers.[26,27] Solid-state copolymerization of DIEDOT monomers with higher reactive DBEDOT monomers was performed, which showed that even a small amount of DBEDOT can significantly accelerate polymerization. The degree of solid-state polymerization with different mass ratios of DIEDOT and DBEDOT monomers at 80 °C was monitored using X-ray diffraction (XRD) (as shown in Figure S1). DIEDOT and DBEDOT have strong and sharp diffraction peaks, revealing relative long-range orders. After copolymerization, a new broad peak appears at approximately 25°, which corresponds to the $\pi-\pi$ stacking in PEDOT. When DIEDOT monomer was taken in larger quantities, the diffraction peaks of the monomers coexisted with those of PEDOT, implying that the monomers were not fully polymerized into PEDOT. When the mass ratio of DIEDOT is less than 50%, the specific diffraction peak belonging to DIEDOT disappears, confirming that the monomer completely polymerizes to form PEDOT. Compared with PEDOT prepared by the homopolymerization of DBEDOT, the peaks in the copolymerization samples shift to a lower position slightly and the intensity decreases, which is mainly due to the I dopant and the excess iodine kinetically trapped in the PEDOT crystal lattice. Even so, both Br- and I-doped PEDOT maintain high crystalline degrees. The polymerization mechanism was proposed, as shown in Figure S2. In the copolymerization process, the byproduct $Br_2$ acts as the catalyst to reduce the energy barrier in the polymerization reaction of DIEDOT, and bromine and iodine generated at the same time act as dopants for the resulting polymers.

Vapor copolymerization of DIEDOT and DBEDOT utilizing our homemade vials was performed, where both monomers were put into the closed vial, and fiber substrates were placed above the monomers (as shown in Figure 1b).



https://doi.org/10.1021/acsomega.1c05717
ACS Omega 2022, 7, 31628−31637

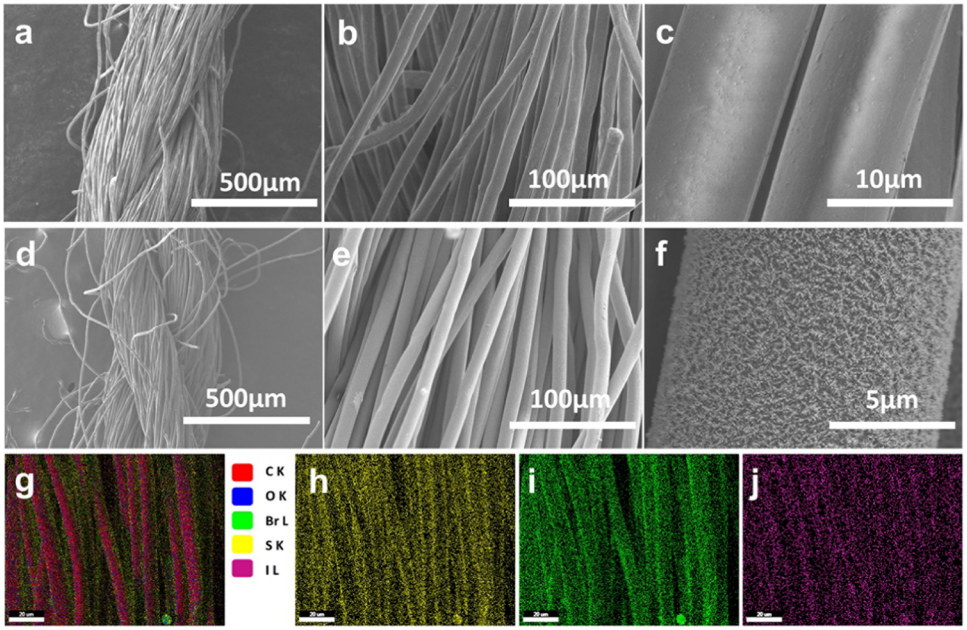


**Figure 2.** SEM images of (a–c) pristine polyester threads and (d–f) PEDOT polyester threads at different magnifications. (g) EDX analysis (elements overlapped) of PEDOT polyester threads. Elemental distribution of (h) S, (i) Br, and (j) I.

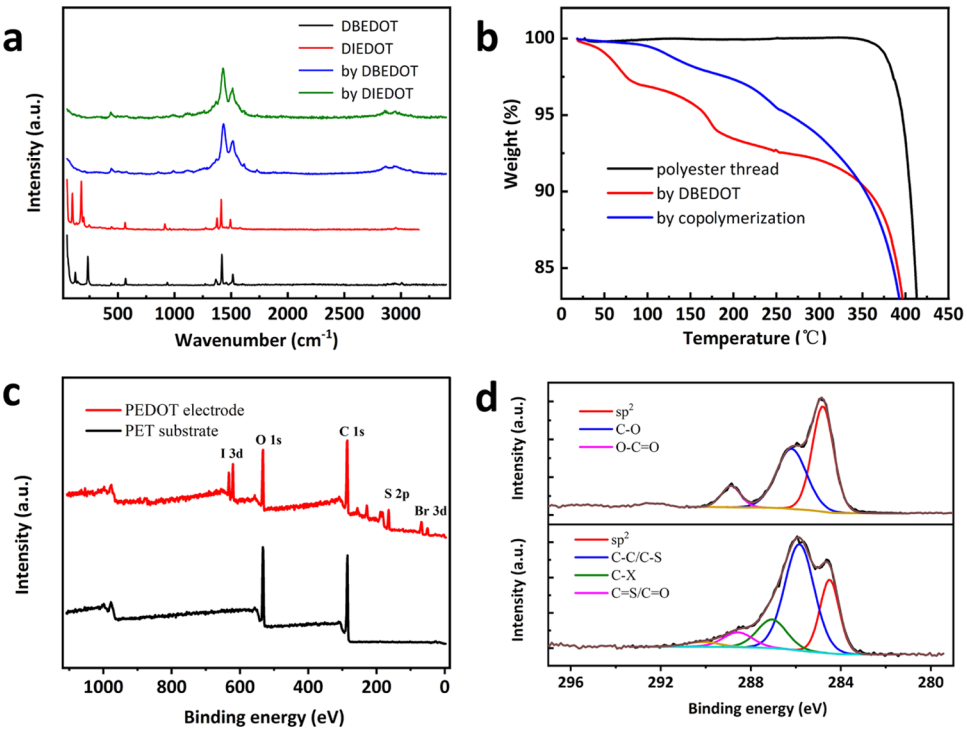


**Figure 3.** (a) Raman spectra of the monomers, polyester substrate, and PEDOT threads. (b) Thermogravimetric analysis (TGA) curves of polyester and PEDOT threads. (c) X-ray photoelectron spectroscopy (XPS) spectra of polyester threads and PEDOT threads and (d) C 1s high-resolution spectra.

The vial was evacuated down to 10 Pa for monomer sublimation and then deposition onto the substrates. The conductivity of PEDOT deposited on planar textile by vapor copolymerization at different monomer mass ratios was investigated, and no noticeable conductivity was observed until the ratio of DIEDOT monomer was reduced to 75% (Figure S3). The samples exhibit the highest conductivity when the ratio of DIEDOT monomer is at 50%. Considering both the conductivity and deposition time, 0.1 g of DIEDOT and 0.1 g of DBDOT monomer are used in the subsequent copolymerization to prepare highly conductive flexible fiber electrodes. Figure 1c shows the photo image and the schematic diagram of a strand of 80 cm-long untreated polyester thread before and after vapor deposition polymerization of PEDOT. The color of the polyester threads obviously changed from white to dark green, demonstrating that PEDOT was formed on the surface of the sewing thread. Due to the high coverage and uniformity of vapor deposition polymerization, PEDOT



https://doi.org/10.1021/acsomega.1c05717
ACS Omega 2022, 7, 31628−31637

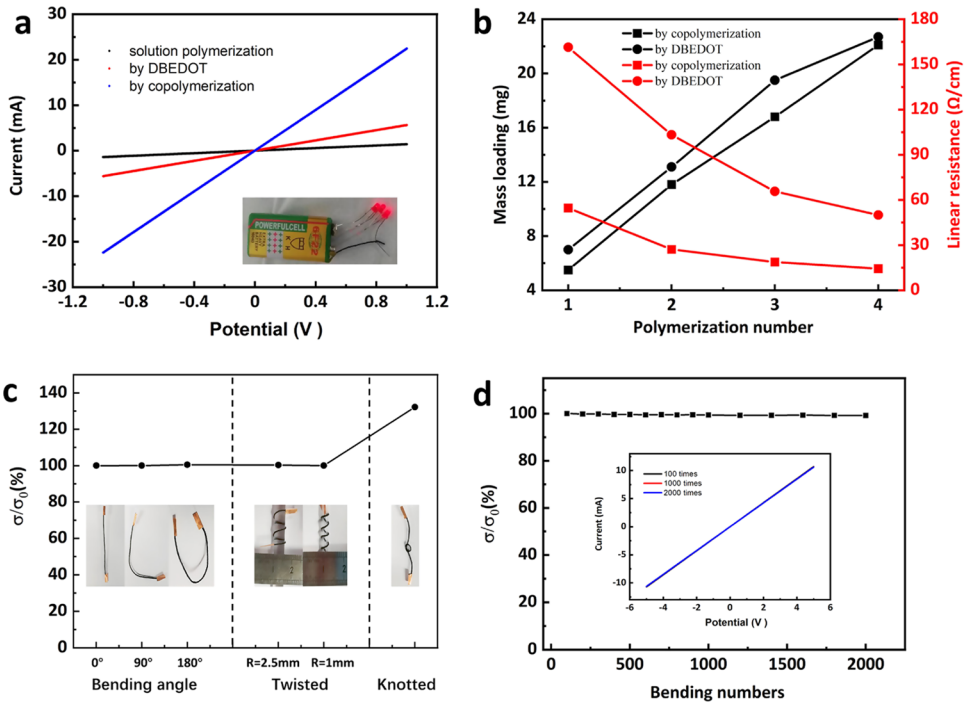


**Figure 4.** (a) Current−voltage curves of PEDOT threads prepared by different methods. (b) Changes in mass loading and linear resistance of PEDOT threads at different times of polymerization. (c) Conductivity retention of the PEDOT thread under various deformations. (d) Conductivity retention of the PEDOT thread under multiple bendings at 180°.

could uniformly wrap the inner thin fiber of the polyester threads. As the process is solvent-free and is initiated by heating, irregular, rough, and nonconductive substrates, such as tissue paper, printing paper, filtering paper, textiles, and even nanostructured $TiO_2$ porous layers, can be modified by a uniform PEDOT layer (as shown in Figures S4 and S5).

The morphologies of the PEDOT-modified polyester thread were characterized using scanning electron microscopy (SEM). Figure 2a−c presents the surface morphology of pristine polyester threads at different magnifications. The thread with a diameter of approximately 600 $\mu$m consists of hundreds of 10 $\mu$m-wide thin fibers, and the surface is flat and smooth. After deposition of PEDOT, the polyester thread retains the multiple strand structure and each thin fiber is uniformly covered by a layer of PEDOT nanograss, as shown in Figure 2d−f. The nanostructured PEDOT can increase the accessibility of the electrolyte and provide more active sites for electrochemical reactions. Energy-dispersive X-ray (EDX) spectroscopy was conducted to present the distribution and the doping state of PEDOT, as shown in Figure 2g−j. The S element could represent the distribution of PEDOT. Both Br and I elements were detected and distributed uniformly on the thin fiber substrates, which means that both elements are introduced into PEDOT as dopants.

To characterize the compositions of PEDOT on the fiber substrate, Raman spectroscopy was conducted at an excitation wavelength of 532 nm. As shown in Figure 3a, DIEDOT and DBEDOT monomers show specific peaks of the thiophene ring in the wavenumber range of 1400−1600 $cm^{-1}$. For the polyester substrate, three main peaks at 1614, 1726, and 1290 $cm^{-1}$ are assigned to the stretching vibration of the aromatic ring, the vibration of the C═O bond, and C−O in ester, respectively. After copolymerization, the PEDOT thread exhibits two remarkable peaks at 1427 and 1513 $cm^{-1}$, which are attributed to the symmetric and asymmetric stretching vibrations of the C═C bond, respectively. PEDOT is also evidenced by the peaks of the C−O−C bond deformation at 437 $cm^{-1}$ and the oxyethylene ring deformation at 987 $cm^{-1}$. The sharp peaks of monomers and the substrate nearly disappeared, which indicates the high polymerization degree and coverage of PEDOT on the substrate. In the enlarged figure, as shown in Figure S6, for PEDOT from copolymerization, the peak of the symmetric stretching vibration of the C═C bond in the thiophene ring is at 1429 $cm^{-1}$ and narrowed. The red shift reveals that the PEDOT resonance structure changes from a mainly coiled benzene structure to a linear or more relaxed quinone structure. The quinone structure has better charge delocalization and a longer conjugation length, and the force between chains could be further increased, which increases the charge mobility and conductivity in PEDOT.[28,29] The narrowed characteristic peak also indicates that the conjugation length of the polymer increases.

To examine the thermal stability of the PEDOT threads, thermogravimetric analysis (TGA) was carried out under nitrogen flow from room temperature (RT) to 400 °C (Figure 3b). Polyester threads show no apparent weight loss before 400 °C. After the deposition of PEDOT, a small percentage of weight is lost at approximately 100 °C, due to the evaporation of the oligomers. In the copolymerization case, the main chain of PEDOT begins to decompose at the temperature range of 215−250 °C, while it is 160−183 °C for the PEDOT threads obtained from the polymerization of DBEDOT. The increased thermostability broadens the application areas of PEDOT and contributes to maintaining the electrochemical property of the resulting devices during usage.

The chemical composition of the PEDOT electrode was analyzed using X-ray photoelectron spectroscopy (XPS). As shown in Figure 3c, the survey spectrum indicates that the


https://doi.org/10.1021/acsomega.1c05717
ACS Omega 2022, 7, 31628−31637

pristine polyester threads are composed of C and O elements. For the PEDOT threads obtained from copolymerization, the new S, Br, and I signals with binding energy at 165, 68, and 620 eV, respectively, were detected, indicating that PEDOT was successfully deposited onto the surface of the polyester fibers. Figure 3d shows that the C 1s core-level spectra of the pristine polyester fiber substrate can be curve-fitted into peaks with binding energies at 288.9, 286.2, and 284.8 eV, which are the typical characteristics of O−C═O, C−O, and $sp^2$ moieties, respectively. After deposition of PEDOT, the peak at 284.5 eV weakened while the peak at 285.84 eV increased, which corresponds to the C−O and C−S moieties in the thiophene ring in the PEDOT chain, respectively. The red shift of the C═C bond (284.5 eV) in the PEDOT electrode indicates the strong $\pi-\pi$ interaction between PEDOT chains.[30] C−Br and C−I at 287.1 eV can be curve-fitted from the spectra, which results from the unreacted terminal groups. Also, the C═S bonds at 288.6 eV were detected from the resonance structure of PEDOT. I $3d_{3/2}$ can be fitted with the peak at 631.1 eV, and the I $3d_{5/2}$ peak was also fitted at 619.7 eV, which proves the introduction of I dopant in the PEDOT system.

To determine the electrical property of the PEDOT fiber electrode prepared by copolymerization of DBEDOT and DIEDOT *via* vapor deposition polymerization, a two-electrode test was carried out by an electrochemical station. For comparison, PEDOT polyester threads were prepared by both solution oxidation polymerization of EDOT and vapor polymerization of DBEDOT. The current−voltage (*IV*) curves of different PEDOT electrodes are shown in Figure 4a. All of the resulting *IV* curves show a typical ohmic behavior, and the linear resistance can be calculated *via* the slope. According to the slopes of the *IV* curves, the conductivity of the PEDOT electrode prepared by copolymerization is higher than those obtained by the other two methods. The calculated linear resistance and electrical conductivity are listed in Table 1. The

**Table 1. Comparison of Conductivity of PEDOT Threads Prepared by Different Methods**

| | by solution polymerization | by DBEDOT | by copolymerization |
|---|---|---|---|
| linear resistance (Ω $cm^{-1}$) | 709 | 178 | 44.6 |
| conductivity (S $cm^{-1}$) | 0.50 | 1.99 | 7.93 |

PEDOT electrode prepared by solution oxidation polymerization has the lowest conductivity of 0.50 S $cm^{-1}$, which is mainly due to the low-mass-loading PEDOT and the poor binding between PEDOT and the substrate. As shown in Figure S7, PEDOT aggregates into particles and is scattered on the substrate, which is the main disadvantage of oxidation polymerization in solution. For the PEDOT electrode by copolymerization, the conductivity is as high as 7.93 S $cm^{-1}$, nearly four times higher than that in the case of polymerization of DBEDOT and 16 times higher than that obtained from oxidation polymerization from solutions. In the inset picture in Figure 4a, three light-emitting diode (LED) bulbs are successfully lighted up when using the PEDOT polyester thread as the conductive connection. Furthermore, the value is also higher than those of composite electrodes based on nonconductive fiber modified by different methods and materials in previous reports in the literature. For example, the linear resistance of PEDOT:PSS-treated cotton fiber is 399 Ω $cm^{-1}$.[31] The conductivity of polypyrrole and carbon black-modified cotton fiber is 12.6 S $m^{-1}$.[32] The conductivity of our composite electrode is even higher than those of some carbon- or metal material-modified nonconductive fibers. The MWCNT-modified cotton fiber exhibits a resistance of 118 Ω $cm^{-1}$.[33] The conductivity of rGO-polyester fiber prepared by multiple coating is 400 Ω $cm^{-1}$.[34] The Cu particle-coated cotton fiber obtained from electroless deposition has a conductivity of 1 S $cm^{-1}$.[35] Therefore, the PEDOT electrode prepared by copolymerization of DBEDOT and DIEDOT not only showed an ordered nanostructure and highly uniform coverage on the substrate but also showed excellent electrical conductivity.

To identify the mass loading of PEDOT and further increase the conductivity of the PEDOT electrode, polymerization was carried out multiple times. Because the mass loading is relatively low, 80 cm-long polyester threads were used as substrates to minimize the weighting error. As shown in Figure 4b, the mass loading of the PEDOT polyester thread prepared by copolymerization is slightly lower than that obtained by DBEDOT polymerization. This also confirms that the improvement in conductivity in copolymerization probably originates from different doping states and polymerization degrees compared with homopolymerization of DBEDOT. The mass loading increases linearly with the number of polymerizations, and the resistance drops dramatically. After four times of copolymerization, the mass loading of the PEDOT polyester thread is about 0.28 mg $cm^{-1}$, while the resistance decreases to 14 Ω $cm^{-1}$, which is much higher than that of DBEDOT polymerization (50 Ω $cm^{-1}$). The tape test was conducted to characterize the adhesion between the PEDOT layer and the PET substrate. As shown in Figure S8a, no active materials fall off the electrode. The conductivity hardly changes after rubbing (Figure S8b), which further confirms the excellent adhesion between the PEDOT layer and the substrates. The PEDOT threads show good stability under common solvents and laundry conditions (Figure S8c).

Figure 4c shows the conductivity retention of PEDOT threads under various bending and twisting conditions. When PEDOT threads are bent to 0, 90, and 180°, the conductivity is almost unchanged. Wrapping PEDOT threads around a glass rod with a small bending radius of 2.5 mm does not reduce the conductivity. Even when the bending radius is reduced to 1 mm, the conductivity of the PEDOT threads remains unaffected. The knotted PEDOT threads show an increase of 32% in conductivity, which is due to the increased contact area of the PEDOT layer at the knot and partial parallel conductive path forms. Since the PEDOT layer is only 200−300 nm thick and interconnects with a uniform film, it shows high flexibility, and the film is not damaged during bending and knotting. As shown in Figure 4d, after 2000 times of bending at 180°, the conductivity of PEDOT threads exhibits no apparent drop, indicating the strong binding between the PEDOT layer and the substrate. The excellent mechanical properties of PEDOT threads meet the needs of wearable electronic devices in practical applications and improve the durability of the devices.

To demonstrate the application of the PEDOT electrode in flexible supercapacitors, $MnO_2$ was then electrodeposited on PEDOT-coated fibers. $MnO_2$ is a widely used capacitive material with high theoretical capacitance, but it suffers from low conductivity and dissolves into solution during cycling. Therefore, another PEDOT layer was deposited *via* vapor deposition polymerization on $MnO_2$ as a protective and conductive layer. For the composite electrode, the $MnO_2$


https://doi.org/10.1021/acsomega.1c05717
ACS Omega 2022, 7, 31628−31637

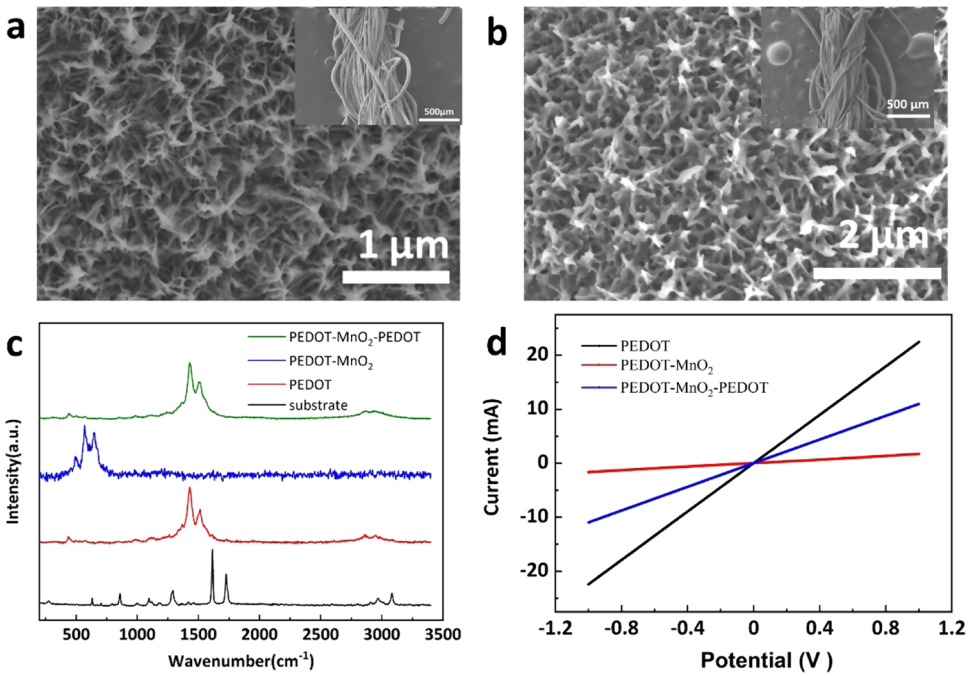


**Figure 5.** SEM images of (a) PEDOT-$MnO_2$ electrode with electrodeposition time of 60 min and (b) PEDOT- $MnO_2$-PEDOT electrode at different magnifications. (c) Raman spectra of the electrode and different composite electrodes. (d) Current−voltage curves of different composite electrodes.

loading content significantly affects the electrochemical performance. Since the mass loading of $MnO_2$ is relatively low, to reduce the weighting error, different deposition times (10, 30, 45, 60, and 75 min) were studied to optimize the specific capacitance of the PM electrode. As shown in Figure S9, $MnO_2$ displays similar nanostructures with increasing electrodeposition time, while the capacitance of the PM electrode increases fast at first and then changes little, as the electrolyte cannot access the thick and compact $MnO_2$ layer (Figure S10). Figure 5a shows the morphology of $MnO_2$ growing on PEDOT polyester thread (PM). $MnO_2$ nanoplates are homogeneously deposited on the thin fibers. EDX mapping analysis in Figure S11 detected Mn element both on the surface and inside the strand of the PEDOT electrode, confirming the uniform distribution of $MnO_2$ on the substrate. Since $MnO_2$ grows on the PEDOT electrode in situ during electrodeposition, it shows good adhesion between $MnO_2$ and the PEDOT layer in the tape test (Figure S12). Figure 5b shows the morphology of the outer PEDOT layer. The nanoplate structure turns into a network structure after deposition of PEDOT, indicating the complete and uniform coverage of PEDOT.

In the Raman spectra in Figure 5c, after electrodeposition of $MnO_2$, the peaks belonging to PEDOT disappeared, and new peaks in the wavenumber range of 500−700 $cm^{-1}$ are observed. The peak at 572 $cm^{-1}$ is ascribed to Mn−O stretching in the basal plane of the MnO6 sheet, and the peak at 653 $cm^{-1}$ is from the MnO6 symmetric stretching vibration, which indicates that $\delta$-$MnO_2$ is obtained.[36,37] For the PMP electrode, the characterized peaks of PEDOT appear again along with the absence of peaks of $MnO_2$, indicating uniform coverage of PEDOT on $MnO_2$. As shown in Figure 5d and Table 2, the conductivity of the PM electrode dramatically decreases to 0.51 S $cm^{-1}$, which is due to the intrinsically poor conductivity of $MnO_2$. After wrapping the outer PEDOT layer, the conductivity of the PEDOT-$MnO_2$-PEDOT (PMP) composite electrode significantly increases to 3.30 S $cm^{-1}$. Consequently, the PEDOT wrapping layer could provide additional conductive paths.

**Table 2. Comparison of Conductivity of Different Composite Electrodes**

| | linear resistance ($\Omega$ $cm^{-1}$) | conductivity (S $cm^{-1}$) |
|---|---|---|
| PEDOT | 44.58 | 7.93 |
| PEDOT-$MnO_2$ | 588.24 | 0.51 |
| PEDOT-$MnO_2$-PEDOT | 91.24 | 3.30 |

To explore the electrochemical behavior of the composite electrode, cyclic voltammetry (CV) and galvanostatic charge−discharge (GCD) were conducted employing a three-electrode configuration. As shown in Figure 6a,b, compared with the PEDOT electrode, the PM electrode shows remarkable improvement in capacitance, owing to the high specific capacitance of $MnO_2$. In the GCD characterization, it is obvious that the outer PEDOT wrapping layer could provide some additional capacitance, since PEDOT is a pseudocapacitance active material as well. Because the outer PEDOT layer is fairly thin (less than 200 nm) and the theoretical specific capacitance of PEDOT (210 F $g^{-1}$) is low, PEDOT only contributes less than 10% of the electrochemical capacitance to the PMP composite electrode. In the GCD curves, the *IR* drop of the PMP electrode is 30% lower that than of the PM electrode, indicating the reduced internal resistance. However, the discharge time of the composite electrodes is slightly longer than the charge time. In the CV curve, there is also an obvious overpotential when the voltage is lower than −0.1 V, indicating some undesirable and irreversible reactions. The CV curves with scan rates ranging from 2 to 200 mV $s^{-1}$ (Figure S13a) and the GCD curves with current densities ranging from 0.3 to 1.8 mA $cm^{-1}$ (Figure S13b) of the PMP electrode were


https://doi.org/10.1021/acsomega.1c05717
ACS Omega 2022, 7, 31628−31637

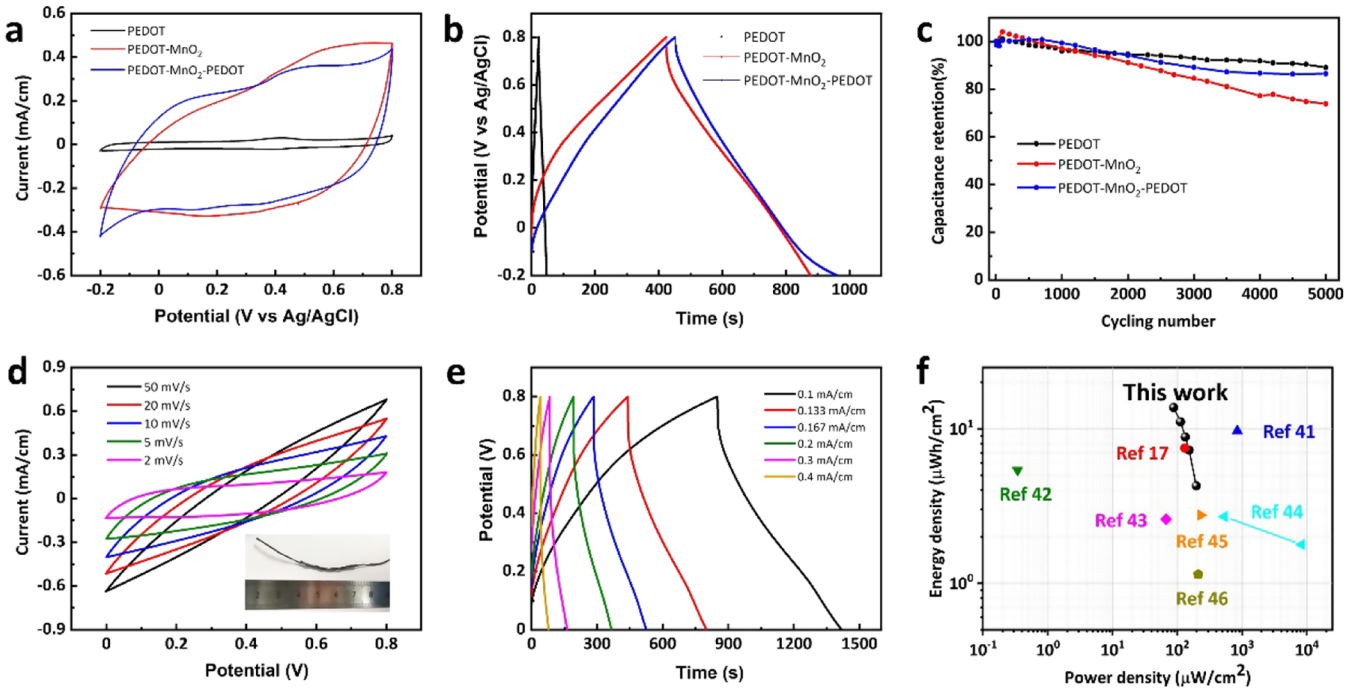


**Figure 6.** Electrochemical performance comparisons of PEDOT, PM, and PMP electrodes. (a) CV curves at the scan rate of 2 mV $s^{-1}$, (b) GCD curves at the current density of 0.3 mA $cm^{-1}$ of different composite electrodes, and (c) cycling performance of the different electrodes during 5000 cycles. Fiber-shaped all-solid-state supercapacitor-based PMP composite electrodes. (d) CV curves at different scan rates (the inset shows the photo of the assembled FSSC), (e) GCD curves at different charge and discharge currents, and (f) Ragone plots compared with other similar reports.

tested. As expected, the electrode displays a high specific capacitance of 157 mF $cm^{-1}$ at a discharge current density of 0.3 mA $cm^{-1}$, corresponding to the areal specific capacitance of 772 mF $cm^{-2}$, which is 1.62 times that of the previously reported composite PEDOT composite electrode based on vapor deposition polymerization of DBEDOT.[25] Based on the GCD curves, the specific capacitance of the composite electrodes at different current densities was calculated, and the results are plotted in Figure S14. The specific capacitance of the PMP electrode is slightly higher than that of the PM electrode at low discharge current densities. As the discharge current density increases, the specific capacitance of the PMP electrode becomes much larger, indicating better rate capability. The enhanced rate capability is attributed to the improvement in electrical conductivity of the electrode after coating another PEDOT layer. Cycling stability was investigated to evaluate the durability of the composite electrodes. As shown in Figure 6c, the PM electrode retained only 74% of the initial capacitance after 5000 times. The capacitance retention of the PMP electrode improves to 86.5%, which confirms that the outer PEDOT layer can protect $MnO_2$ from structurally collapsing or peeling off into the electrolyte during long-time cycling. The PMP composite electrode also shows superior flexibility because of the highly flexible substrate electrode. As shown in Figure S15, the CV curves of the composite electrode remain nearly unchanged at different bending angles or when twisted and knotted.

The symmetric fiber-shaped solid-state supercapacitors (FSSCs) based on PMP composite electrodes were assembled using PVA/LiCl gel as electrolyte. The FSSCs have a stable potential window from 0 to 0.8 V in the CV curve (Figure 6d). GCD tests at various discharge current densities were also conducted, as shown in Figure 6e. Based on the GCD curve, the linear specific capacitance of the whole device was calculated to be 79.3 mF $cm^{-1}$ at a current density of 0.1 mA $cm^{-1}$, with the corresponding areal specific capacitance and volumetric capacitance of 192.3 mF $cm^{-2}$ and 12.0 F $cm^{-3}$, respectively. The specific capacitance is higher than that of many fiber supercapacitors reported in the literature.[38−41] To represent the relationship between energy density and power density, the Ragone plot was obtained from GCD curves and compared with other reported representative works (Figure 6f). The as-prepared FSSC delivered the highest energy density of 13.8 $\mu$Wh $cm^{-2}$ (linear energy density of 5.6 $\mu$Wh $cm^{-1}$ and volumetric energy density of 0.85 mWh $cm^{-3}$) and a power density of 87.4 $\mu$W $cm^{-2}$ (linear power density of 35.7 $\mu$W $cm^{-1}$ and volumetric power density of 5.4 mW $cm^{-3}$) at a current density of 0.1 mA $cm^{-1}$. The electrochemical performance is superior to reported FSSCs based on natural textile electrodes (cotton or PET fiber) or $MnO_2$ active material, such as PPy/MO/Cotton,[17] Cotton/Graphene/PANI yarn,[41] PET/Au/Ni-MOF@carbon yarns,[42] CNT/$MnO_2$/Nylon,[43] carbon fiber/$MnO_2$,[4444] $MnO_2$-CNT-G-Ni,[45] and $MnO_2$/CNT.[46] The excellent electrochemical performance and mechanical flexibility of PMP electrodes and corresponding fiber-shaped devices provide great application potential in wearable electronics.

## 3. CONCLUSIONS

In summary, iodine-substituted EDOT was synthesized and copolymerized with DBEDOT *via* vapor deposition polymerization to fabricate highly flexible and conductive PEDOT polyester threads, the conductivity of which was four times higher than that obtained when homopolymerized from DBEDOT alone. We used it as a current collector and modified it with $MnO_2$ to fabricate fiber-shaped electrodes,


https://doi.org/10.1021/acsomega.1c05717
ACS Omega 2022, 7, 31628−31637

showing linear specific capacitance of 157 mF $cm^{-1}$ and areal specific capacitance of 772 mF $cm^{-2}$. The composite electrode also exhibits superior rate capability, long cycling life, and mechanical flexibility. FSSCs based on the composite electrode were assembled and showed superior electrochemical performance. This work provides a facile method to fabricate high-conductivity flexible fiber electrodes for supercapacitors, which have potential applications in wearable electronics.

## 4. EXPERIMENTAL SECTION

**4.1. Materials.** EDOT (98%) was purchased from Shanghai Yuanye Bio-Technology Co., Ltd. *N*-bromosuccinimide (99%) and *N*-iodosuccinimide (99%) were purchased from Shanghai Macklin Biochemical Co., Ltd. Chloroform, acetic acid (98%), and $Na_2CO_3$ were purchased from Beijing Tong Guang Fine Chemical Company. Polyester threads were purchased from Changshu Hengze Textile Co., Ltd. All materials were used as received without further purification.

**4.2. Synthesis of DBEDOT and DIEDOT.** Briefly, 7.2 g of *N*-bromosuccinimide was dissolved in 60 mL of $CHCl_3$ and 30 mL of acetic acid. The Schlenk line was used to exchange the air with $N_2$ and keep the inert atmosphere in the reactor. The resulting mixture was kept in the dark to avoid light and in an ice bath to maintain the temperature. Then, 2.8 g of EDOT was added to the solution. The mixture was stirred for 2 h and quenched with water. The water layer was extracted using chloroform. Then, 5 wt % $Na_2CO_3$ was used to neutralize the combined organic phase. The organic solvent was concentrated using a rotary evaporator. The solid product was recrystallized using ethanol as solvent.

Briefly, 9.39 g of *N*-iodosuccinimide was dissolved in 60 mL of $CHCl_3$ and 30 mL of acetic acid. The Schlenk line was used to exchange the air with $N_2$ and keep the inert atmosphere in the reactor. The resulting mixture was kept in the dark to avoid light and in an ice bath to maintain the temperature. Then, 2.8 g of EDOT was added to the solution. The mixture was stirred for 2 h and quenched with water. The white precipitate was filtered and washed with cold ethanol. The product was further purified using column chromatography.

**4.3. Preparation of PEDOT Polyester Threads.** PEDOT polyester threads were synthesized *via* vapor deposition polymerization. Briefly, 0.2 g of DBEDOT and the polyester thread substrate were put into a sealed vial. The system was evacuated and heated in an oven at 80 °C for 24 h. For the copolymerization case, a total of 0.2 g of DBEDOT and DIEDOT with different mass ratios used as monomers was taken, while the other conditions were kept the same.

**4.4. Preparation of PEDOT-$MnO_2$ Polyester Thread Composite Electrodes.** The $MnO_2$ nanoplatelet array was synthesized through a constant voltage electrodeposition method in a three-electrode system. The PEDOT polyester thread, Ag/AgCl, and platinum were used as the working electrode, reference electrode, and counter electrode, respectively. The deposition voltage was set at 0.75 V in 100 mL of an aqueous solution containing 0.05 M manganese acetate and 0.02 M ammonium acetate at room temperature for different deposition times. The composite electrodes were washed with deionized water and dried in an oven at 60 °C.

**4.5. Preparation of PEDOT-$MnO_2$-PEDOT Polyester Thread Composite Electrodes.** Briefly, 0.1 g of DBEDOT and PEDOT-$MnO_2$ polyester threads were placed in a sealed vial. The system was evacuated and heated in an oven at 80 °C for 24 h.

**4.6. Fabrication of the Flexible Solid-State Supercapacitor.** Specifically, 5 g of PVA and 50 mL of LiCl solution (1.0 M) were mixed and heated at 90 °C under stirring until a homogeneous solution of PVA-LiCl gel electrolyte was formed. Two identical PEDOT/$MnO_2$/PEDOT electrodes were coated with PVA-LiCl gel electrolyte, dried under ambient conditions, and then twisted together, and the solid-state FSSC was obtained finally.

**4.7. Characterization and Electrochemical Measurement.** The morphology and composition of the electrodes were characterized using field-emission scanning electron microscopy (FE-SEM, Hitachi S-4800), energy-dispersive X-ray (EDX, Hitachi S-4800) spectroscopy, micro-Raman imaging spectroscopy (DXRxi), and a one-dimensional X-ray diffractometer (X pert pro). Electrochemical cyclic voltammetry, galvanostatic charge−discharge measurements, and electrochemical impedance spectroscopy (EIS) were conducted using Metrohm Autolab electrochemical workstation. The electrochemical properties were investigated in 1 mol $L^{-1}$ $Na_2SO_4$ solution using a three-electrode system, where the composite fiber electrode, Ag/AgCl, and platinum were used as the working electrode, reference electrode, and counter electrode, respectively.

**4.8. Calculation of Specific Capacitance, Energy Density, and Power Density.** The linear specific capacitance was calculated from the galvanostatic charge−discharge curves using the following equation

$$C = \frac{Q}{l \times \Delta V} = \frac{\int I\,dt}{l \times \Delta V} = \frac{I}{l} \times \frac{\Delta t}{(V - I \times R_{drop})}$$

where $C$ (F $m^{-1}$) is the linear specific capacitance, $I$ (A) is the discharge current, $\Delta V$ (V) is the discharge potential range, $IR_{drop}$ is the voltage drop at the beginning of the discharge, $\Delta t$ (s) is the discharge time, and $l$ (m) is the active length.

The surface area and volume of the composite were calculated according to the equations $S = 2\pi dl$ and $V = 2\pi r^2 l$, where $d$ ($d$ = 650 $\mu$m) and $r$ ($r$ = 325 $\mu$m) are the diameter and radius of the PEDOT-$MnO_2$-PEDOT composite electrode, respectively, and $l$ is the active length. The areal specific capacitance (F $cm^{-2}$) and the volumetric specific capacitance (F $cm^{-3}$) are calculated in the same as the linear specific capacitance.

## ■ ASSOCIATED CONTENT

### Supporting Information

The Supporting Information is available free of charge at https://pubs.acs.org/doi/10.1021/acsomega.1c05717.

Polymerization mechanism and PEDOT deposited on different substrates and the electrochemical test of the PEDOT electrode and the $MnO_2$-based composite electrodes (PDF)

## ■ AUTHOR INFORMATION

### Corresponding Authors

**Shaocong Hou** − *School of Electrical Engineering and Automation, Wuhan University, Wuhan 430072, China*; Email: sc.hou@whu.edu.cn

**Dechun Zou** − *Beijing National Laboratory for Molecular Sciences, Key Laboratory of Polymer Chemistry and Physics of Ministry of Education, Center for Soft Matter Science and Engineering, College of Chemistry and Molecular Engineering*



https://doi.org/10.1021/acsomega.1c05717
*ACS Omega* 2022, 7, 31628−31637

*and Beijing Engineering Research Center for Active Matrix Display, Peking University, Beijing 100871, China;* orcid.org/0000-0001-8241-4992; Email: dczou@pku.edu.cn

### Authors

**Jing Hu** − *Beijing National Laboratory for Molecular Sciences, Key Laboratory of Polymer Chemistry and Physics of Ministry of Education, Center for Soft Matter Science and Engineering, College of Chemistry and Molecular Engineering, Peking University, Beijing 100871, China*

**Bo Gao** − *Beijing National Laboratory for Molecular Sciences, Key Laboratory of Polymer Chemistry and Physics of Ministry of Education, Center for Soft Matter Science and Engineering, College of Chemistry and Molecular Engineering, Peking University, Beijing 100871, China*

**Qi Qi** − *Beijing National Laboratory for Molecular Sciences, Key Laboratory of Polymer Chemistry and Physics of Ministry of Education, Center for Soft Matter Science and Engineering, College of Chemistry and Molecular Engineering, Peking University, Beijing 100871, China*

**Zhuang Zuo** − *Beijing National Laboratory for Molecular Sciences, Key Laboratory of Polymer Chemistry and Physics of Ministry of Education, Center for Soft Matter Science and Engineering, College of Chemistry and Molecular Engineering, Peking University, Beijing 100871, China*

**Kai Yan** − *Zhejiang Huacai Testing Technology Co., Ltd, Hangzhou 310012, China*

Complete contact information is available at: https://pubs.acs.org/10.1021/acsomega.1c05717

### Notes

The authors declare no competing financial interest.

## ■ ACKNOWLEDGMENTS

This work is jointly supported by the National Natural Science Foundation of China (Grant Nos. 52073002, 51773003, and 51711540302) and the National Key Research and Development Program of China (Grant No. 2020YFB1506400).

## ■ REFERENCES

(1) Lu, C.; Chen, X. Latest advances in flexible symmetric supercapacitors: From material engineering to wearable applications. *Acc. Chem. Res.* **2020**, *53*, 1468−1477.

(2) Liu, Z.; Mo, F.; Li, H.; Zhu, M.; Wang, Z.; Liang, G.; Zhi, C. Advances in flexible and wearable energy-storage textiles. *Small Methods* **2018**, *2*, No. 1800124.

(3) Dubal, D. P.; Chodankar, N. R.; Kim, D. H.; Gomez-Romero, P. Towards flexible solid-state supercapacitors for smart and wearable electronics. *Chem. Soc. Rev.* **2018**, *47*, 2065−2129.

(4) Huang, Q.; Wang, D.; Zheng, Z. Textile-based electrochemical energy storage devices. *Adv. Energy Mater.* **2016**, *6*, No. 1600783.

(5) Chen, D.; Jiang, K.; Huang, T.; Shen, G. Recent advances in fiber supercapacitors: materials, device configurations, and applications. *Adv. Mater.* **2020**, *32*, No. 1901806.

(6) Lee, J.; Llerena Zambrano, B.; Woo, J.; Yoon, K.; Lee, T. Recent advances in 1D stretchable electrodes and devices for textile and wearable electronics: Materials, fabrications, and applications. *Adv. Mater.* **2019**, *32*, No. 1902532.

(7) Cai, X.; Peng, M.; Yu, X.; Fu, Y.; Zou, D. Flexible planar/fiber-architectured supercapacitors for wearable energy storage. *J. Mater. Chem. C* **2014**, *2*, 1184−1200.

(8) Nagaraju, G.; Sekhar, S. C.; Yu, J. S. Utilizing waste cable wires for high-performance fiber-based hybrid supercapacitors: an effective approach to electronic-waste management. *Adv. Energy Mater.* **2018**, *8*, No. 1702201.

(9) Niu, X.; Zhu, G.; Yin, Z.; Dai, Z.; Hou, X.; Shao, J.; Huang, W.; Zhang, Y.; Dong, X. Fiber-based all-solid-state asymmetric supercapacitors based on $Co_3O_4$@$MnO_2$ core/shell nanowire arrays. *J. Mater. Chem. A* **2017**, *5*, 22939−22944.

(10) Sun, J.; Huang, Y.; Fu, C.; Huang, Y.; Zhu, M.; Tao, X.; Zhi, C.; Hu, H. A high performance fiber-shaped PEDOT@$MnO_2$//C@$Fe_3O_4$ asymmetric supercapacitor for wearable electronics. *J. Mater. Chem. A* **2016**, *4*, 14877−14883.

(11) Wang, K.; Meng, Q.; Zhang, Y.; Wei, Z.; Miao, M. High-performance two-ply yarn supercapacitors based on carbon nanotubes and polyaniline nanowire arrays. *Adv. Mater.* **2013**, *25*, 1494−1498.

(12) Xu, T.; Zhang, Z.; Qu, L. Graphene-based fibers: Recent advances in preparation and application. *Adv. Mater.* **2020**, *32*, No. 1901979.

(13) Liu, W.; Liu, N.; Shi, Y.; Chen, Y.; Yang, C.; Tao, J.; Wang, S.; Wang, Y.; Su, J.; Li, L.; Gao, Y. A wire-shaped flexible asymmetric supercapacitor based on carbon fiber coated with a metal oxide and a polymer. *J. Mater. Chem. A* **2015**, *3*, 13461−13467.

(14) Wen, J.; Xu, B.; Gao, Y.; Li, M.; Fu, H. Wearable technologies enable high-performance textile supercapacitors with flexible, breathable and wearable characteristics for future energy storage. *Energy Storage Mater.* **2021**, *37*, 94−122.

(15) Liu, L.; Yu, Y.; Yan, C.; Li, K.; Zheng, Z. Wearable energy-dense and power-dense supercapacitor yarns enabled by scalable graphene-metallic textile composite electrodes. *Nat. Commun.* **2015**, *6*, No. 7260.

(16) Liu, N.; Ma, W.; Tao, J.; Zhang, X.; Su, J.; Li, L.; Yang, C.; Gao, Y.; Golberg, D.; Bando, Y. Cable-type supercapacitors of three-dimensional cotton thread based multi-grade nanostructures for wearable energy storage. *Adv. Mater.* **2013**, *25*, 4925−4931.

(17) Wei, C.; Xu, Q.; Chen, Z.; Rao, W.; Fan, L.; Yuan, Y.; Bai, Z.; Xu, J. An all-solid-state yarn supercapacitor using cotton yarn electrodes coated with polypyrrole nanotubes. *Carbohydr. Polym.* **2017**, *169*, 50−57.

(18) Yu, Z.; Li, C.; Abbitt, D.; Thomas, J. Flexible, sandwich-like Ag-nanowire/PEDOT:PSS-nanopillar/$MnO_2$ high performance supercapacitors. *J. Mater. Chem. A* **2014**, *2*, 10923−10929.

(19) Wang, Z.; Tammela, P.; Huo, J.; Zhang, P.; Stromme, M.; Nyholm, L. Solution-processed poly(3,4-ethylenedioxythiophene) nanocomposite paper electrodes for high-capacitance flexible supercapacitors. *J. Mater. Chem. A* **2016**, *4*, 1714−1722.

(20) Ala, O.; Hu, B.; Li, D.; Yang, C.-L.; Calvert, P.; Fan, Q. Conductive textiles via vapor-phase polymerization of 3,4-ethylenedioxythiophene. *ACS Appl. Mater. Interfaces* **2017**, *9*, 29038−29046.

(21) Zhang, L.; Fairbanks, M.; Andrew, T. L. Rugged textile electrodes for wearable devices obtained by vapor coating off-the-shelf, plain-woven fabrics. *Adv. Funct. Mater.* **2017**, *27*, No. 1700415.

(22) Meng, H.; Perepichka, D. F.; Wudl, F. Facile solid-state synthesis of highly conducting poly(ethylenedioxythiophene). *Angew. Chem., Int. Ed.* **2003**, *42*, 658−661.

(23) Meng, H.; Perepichka, D. F.; Bendikov, M.; Wudl, F.; Pan, G. Z.; Yu, W.; Dong, W.; Brown, S. Solid-state synthesis of a conducting polythiophene via an unprecedented heterocyclic coupling reaction. *J. Am. Chem. Soc.* **2003**, *125*, 15151−15162.

(24) Yu, X.; Su, X.; Yan, K.; Hu, H. W.; Peng, M.; Cai, X.; Zou, D. C. Stretchable, conductive, and stable PEDOT-modified textiles through a novel in situ polymerization process for stretchable supercapacitors. *Adv. Mater. Technol.* **2016**, *1*, No. 1600009.

(25) Gao, X.; Xiao, X.; Dong, B.; Hu, J.; Tang, S.; Qi, W.; Zou, D. Converting commercial sewing threads into high-performance and flexible/wearable fiber-shaped supercapacitors via facile vapor deposition polymerization. *ChemistrySelect* **2019**, *4*, 5355−5365.

(26) Lee, S.; Gleason, K. K. Enhanced optical property with tunable band gap of cross-linked PEDOT copolymers via oxidative chemical vapor deposition. *Adv. Funct. Mater.* **2015**, *25*, 85−93.

(27) Kayser, L. V.; Russell, M. D.; Rodriquez, D.; Abuhamdieh, S. N.; Dhong, C.; Khan, S.; Stein, A. N.; Ramirez, J.; Lipomi, D. J. RAFT polymerization of an intrinsically stretchable water-soluble block copolymer scaffold for PEDOT. *Chem. Mater.* **2018**, *30*, 4459−4468.
(28) Wu, F.; Li, P.; Sun, K.; Zhou, Y.; Chen, W.; Fu, J.; Li, M.; Lu, S.; Wei, D.; Tang, X.; Zang, Z.; Sun, L.; Liu, X.; Ouyang, J. Conductivity enhancement of PEDOT:PSS via addition of chloroplatinic acid and its mechanism. *Adv. Electron. Mater.* **2017**, *3*, No. 1700047.
(29) Ouyang, J.; Chi, C. W.; Chen, F. C.; Xi, Q. F.; Yang, Y. High-conductivity poly (3,4-ethylenedioxythiophene): poly(styrene sulfonate) film and its application in polymer optoelectronic devices. *Adv. Funct. Mater.* **2005**, *15*, 203−208.
(30) Du, F.-P.; Cao, N.-N.; Zhang, Y.-F.; Fu, P.; Wu, Y.-G.; Lin, Z.-D.; Shi, R.; Amini, A.; Cheng, C. PEDOT:PSS/graphene quantum dots films with enhanced thermoelectric properties via strong interfacial interaction and phase separation. *Sci. Rep.* **2018**, *8*, No. 6441.
(31) Ma, Y.; Wang, Q.; Liang, X.; Zhang, D.; Miao, M. Wearable supercapacitors based on conductive cotton yarns. *J. Mater. Sci.* **2018**, *53*, 14586−14597.
(32) Villanueva, R.; Ganta, D.; Guzman, C. Mechanical, in-situ electrical and thermal properties of wearable conductive textile yarn coated with polypyrrole/carbon black composite. *Mater. Res. Express* **2019**, *6*, No. 016307.
(33) Shim, B. S.; Chen, W.; Doty, C.; Xu, C.; Kotov, N. A. Smart electronic yarns and wearable fabrics for human biomonitoring made by carbon nanotube coating with polyelectrolytes. *Nano Lett.* **2008**, *8*, 4151−4157.
(34) Yue, Y.; Yang, S.-Y.; Huang, Y.-L.; Sun, B.; Bian, S.-W. Reduced graphene oxide/polyester yarns supported conductive metal-organic framework nanorods as novel electrodes for all-solid-state supercapacitors. *Energy Fuels* **2020**, *34*, 16879−16884.
(35) Liu, X.; Chang, H.; Li, Y.; Huck, W. T. S.; Zheng, Z. Polyelectrolyte-bridged metal/cotton hierarchical structures for highly durable conductive yarns. *ACS Appl. Mater. Interfaces* **2010**, *2*, 529−535.
(36) Xia, H.; Wang, Y.; Lin, J.; Lu, L. Hydrothermal synthesis of $MnO_2$/CNT nanocomposite with a CNT core/porous $MnO_2$ sheath hierarchy architecture for supercapacitors. *Nanoscale Res. Lett.* **2012**, *7*, No. 33.
(37) Chen, H.; Wang, Y.; Lv, Y.-K. Catalytic oxidation of NO over $MnO_2$ with different crystal structures. *RSC Adv.* **2016**, *6*, 54032−54040.
(38) Xu, Y. F.; Yan, Y. S.; Lu, W. B.; Yarlagadda, S.; Xu, G. B. A. High-performance flexible asymmetric fiber-shaped supercapacitor based on CF/PPy and CNT/$MnO_2$ composite electrodes. *ACS Appl. Energy Mater.* **2021**, *4*, 10639−10645.
(39) Huang, Y.; Hu, H.; Huang, Y.; Zhu, M. S.; Meng, W. J.; Liu, C.; Pei, Z. X.; Hao, C. L.; Wang, Z. K.; Zhi, C. Y. From industrially weavable and knittable highly conductive yarns to large wearable energy storage textiles. *ACS Nano* **2015**, *9*, 4766−4775.
(40) Xu, Q.; Fan, L. L.; Yuan, Y.; Wei, C. Z.; Bai, Z. K.; Xu, J. All-solid-state yarn supercapacitors based on hierarchically structured bacterial cellulose nanofiber-coated cotton yarns. *Cellulose* **2016**, *23*, 3987−3997.
(41) Jin, C.; Wang, H. T.; Liu, Y. N.; Kang, X. H.; Liu, P.; Zhang, J. N.; Jin, L. N.; Bian, S. W.; Zhu, Q. High-performance yarn electrode materials enhanced by surface modifications of cotton fibers with graphene sheets and polyaniline nanowire arrays for all-solid-state supercapacitors. *Electrochim. Acta* **2018**, *270*, 205−214.
(42) Yang, S.-Y.; Wang, Y.-F.; Yue, Y.; Bian, S.-W. Flexible polyester yarn/Au/conductive metal-organic framework composites for yarn-shaped supercapacitors. *J. Electroanal. Chem.* **2019**, *847*, No. 113218.
(43) Choi, C.; Kim, S. H.; Sim, H. J.; Lee, J. A.; Choi, A. Y.; Kim, Y. T.; Lepro, X.; Spinks, G. M.; Baughman, R. H.; Kim, S. J. Stretchable, weavable coiled carbon nanotube/$MnO_2$/polymer fiber solid-state supercapacitors. *Sci. Rep.* **2015**, *5*, No. 9387.
(44) Noh, J.; Yoon, C.-M.; Kim, Y. K.; Jang, J. High performance asymmetric supercapacitor twisted from carbon fiber/$MnO_2$ and carbon fiber/$MoO_3$. *Carbon* **2017**, *116*, 470−478.
(45) Kang, Q.; Zhao, J.; Li, X.; Zhu, G.; Feng, X.; Ma, Y.; Huang, W.; Liu, J. A single wire as all-inclusive fully functional supercapacitor. *Nano Energy* **2017**, *32*, 201−208.
(46) Xu, P.; Wei, B.; Cao, Z.; Zheng, J.; Gong, K.; Li, F.; Yu, J.; Li, Q.; Lu, W.; Byun, J.-H.; Kim, B.-S.; Yan, Y.; Chou, T.-W. Stretchable wire-shaped asymmetric supercapacitors based on pristine and $MnO_2$ coated carbon nanotube fibers. *ACS Nano* **2015**, *9*, 6088−6096.


https://doi.org/10.1021/acsomega.1c05717
*ACS Omega* 2022, 7, 31628−31637